Journal of Materials Chemistry A

Accepted Manuscript

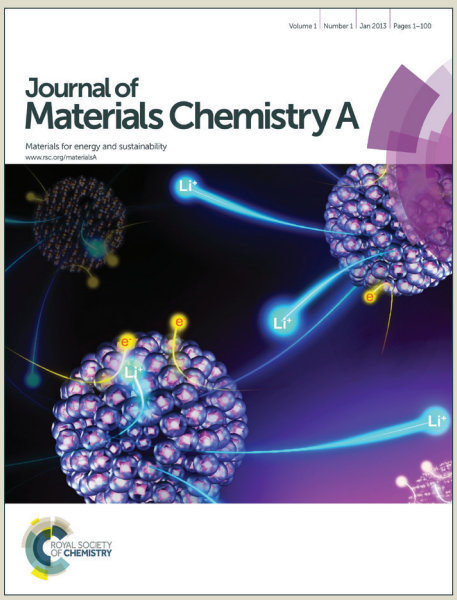

ROYAL SOCIETY OF CHEMISTRY

www.rsc.org/materialsA

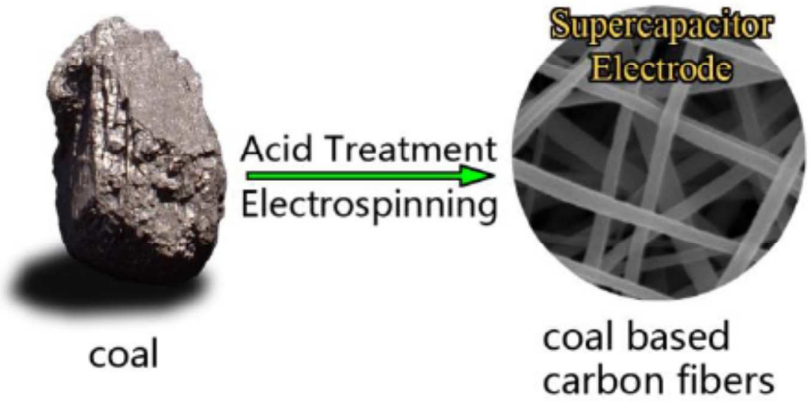

Porous carbon nanofibers were prepared by electrospinning using coal as the raw material. The activated carbon fiber mat is a promising candidate for the electrode of supercapacitors.

Cite this: DOI: 10.1039/c0xx00000x

www.rsc.org/xxxxxx

ARTICLE TYPE

Coal based activated carbon nanofibers prepared by electrospinning

Hongyang Zhao [a], Luxiang Wang [a], Dianzeng Jia*[a], Wei Xia[b], Jun Li [a] , Zaiping Guo[c]

Received (in XXX, XXX) Xth XXXXXXXXX 20XX, Accepted Xth XXXXXXXXX 20XX
DOI: 10.1039/b000000x

Coal based nanofibers were prepared by electrospinning a mixture of polyacrylonitrile and acid treated coal. Coal based activated carbon fibers were further obtained by carbonization and steam activation. The effects of acid treatment on raw coal were studied to explain the enhanced solubility in various solvents. The solubility of coal was as high as 6.6wt% in N, N-dimethylformamide. The electrochemical performance of supercapacitor electrode using the coal based activated carbon fiber mat was then studied. This binder-free electrode showed a specific capacitance of 230 F g^{-1} at a current density of 1 A g^{-1}, and excellent capacity retention of 97% after 1000 cycles.

Introduction

Increasing energy consumption in both industry and everyday life has motivated people to find efficient ways to produce and store energy. As one of the most commonly used traditional fuels, coal has been an indispensable energy resource for thousands of years. Coal has been most commonly used in cooking, heating, and the production of electricity. Over the last 100 years, with the depletion of coal resources, people developed several ways to improve the utilization rate of coal. For instance, liquefaction and gasification have played major roles in converting coal into liquid or gaseous fuel. Besides energy production, coal can be used as an energy storage material as well. Activated carbon based on coal is an ideal candidate for supercapacitors due to its large specific surface area (SSA), high conductivity, and low cost[1]. Activated carbon is not entirely electrochemically inert. On the one hand, the large SSA of activated carbon contributes to electric double layer (EDL) capacitance. On the other hand, the surface oxygen groups contribute to the pseudocapacitance derived from the fast redox Faradic reaction between the electrolyte and the electroactive species on the electrode surface[2]. The type of activated carbon has a great influence on the assembly and performance of the supercapacitor. Powders with high SSA are usually inconvenient for the fabrication of electrode structures with good integrity[3], while fibrous activated carbon is preferred because of its convenience in fabricating electrodes and hierarchical porous structure for efficient ion diffusion[4].

Activated carbon fibres (ACFs), with both fibrous structure and large SSA, have been seen as a promising electrode material for lithium ion batteries[5-10] and supercapacitors[11]. Various activation processes, such as physical and chemical activation, share the principle of eliminating the reactive carbon from the structure at high temperature, thus forming pores[11]. In order to enhance electrolyte transportation and to increase SSA, fibres with smaller diameters are preferred. Electrospinning, a technology that has long been adopted to prepare fibres on the nanoscale, is an easy way to prepare ACF supercapacitor electrodes. The resultant ACF mat can be readily used as supercapacitor electrode, as it needs no binder or conductive agent. This simplifies the electrode assembly process. Furthermore, the ACF mat is inherently suitable for fabricating flexible energy storage devices.

There is a wide range of raw materials for ACFs. Natural fibrous materials such as bacterial cellulose[12], egg shell membrane[13], and silk cocoon[14] have been used to make electrode material. Man-made fibrous carbon materials for supercapacitors are mainly derived from cotton fibers[15], pitch-based carbon fibers[16], and polyacrylonitrile (PAN) fibers[17]. Coal, as a traditional material for activated carbon electrode, needs to be broken down to the nanoscale by a low energy consumption method for a wider range of application. According to the reports in the literature, carbon nanotubes or carbon nanofibers derived from coal can only be achieved by arc-discharge[18] or arc-plasma-assisted chemical vapour deposition[19]. Both of these methods are energy hungry and inconvenient for operation. Compared with these methods, electrospinning is a method with low energy consumption. Furthermore, electrospinning is a much easier method in terms of operation, and can produce fibres with controlled morphology, such as branched hierarchical structures[20], porous fibres, single-walled or multi-walled nanotubes, and multichannel fibers[21]. It is worth investigating whether fibrous carbon nanomaterials based on coal can be achieved by electrospinning. As far as we know, however, there are few reports on this aspect. In the present work, we report a method to prepare supercapacitor electrode material based on coal by electrospinning. The coal based activated carbon nanofibers (CBACFs) were fabricated into a binder-free supercapacitor electrode, and they showed promising electrochemical performance.

Experimental

Spinning dope preparation

Coal was obtained from Dahuangshan, Xinjiang, China, An industrial analysis of the raw coal components is shown in Table 1. PAN, N, N-dimethylformamide (DMF), H_2SO_4, and HNO_3 were purchased commercially and used without further purification. Firstly, the coal was pulverized and sieved with a 200 mesh standard sieve. Then, 10 g of the fine black powders were carefully added into a flask containing 500 mL of a mixture of HNO_3 (63%) and H_2SO_4 (98%) (1:3, volume ratio) in an ice bath in order to absorb the heat generated during the reaction. The flask was left overnight and diluted with deionized water. The obtained product was vacuum filtrated and washed with deionized water several times until the pH value approached neutral. Finally, dark brown powders were obtained. The PAN solution was prepared by adding 20 mL DMF into a scintillation flask containing 1.0 g PAN, and then the mixture was heated to 70°C and stirred until a transparent solution was obtained. Afterwards, a certain amount of acid treated coal (0.2 g, 0.6 g, 1.0 g) was added into the solution and stirred overnight. The homogenous black viscous solution that resulted was then left overnight. The upper part of the solution was used as the spinning dope in order to prevent the insoluble minerals from blocking the needle during spinning.

Table 1 - Component analysis of raw coal.

Proximate analysis(wt%)			Ultimate analysis (wt%)				
M_{ad}	A_d	V_{daf}	C_d	H_d	O_d	N_d	$S_{t,d}$
1.22	7.18	48.34	63.17	3.63	14.30	1.11	0.20

Electrospinning

The electrospinning process was performed on a conventional electrospinning set-up. A 10 mL syringe connected to a stainless needle with inner diameter of 0.5 mm was linked to a high voltage power supply at 20 kV (Dongwen, Tianjin). No syringe pump was used during the spinning process. A piece of graphite paper was used as the collector. The distance between the spinneret and the collector was kept at 20 cm. A 275 W heat lamp was used to keep the temperature of the spinning environment around 40°C.

Carbonization and activation of fibers

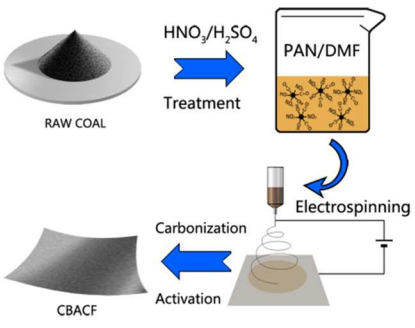

Fig. 1 Schematic illustration of synthesis of coal-based carbon activated nanofibers.

The obtained PAN/coal composite mat was firstly pre-oxidized in air at 280°C for 3 h, with the heating rate 1°Cmin^{-1}. The composite mat was fixed on a ceramic boat with two steel clips in order to maintain tension during the pre-oxidation. Then, the mat was mounted in a tube furnace, ramped to 800°C at the heating rate of 5°Cmin^{-1} under argon atmosphere, and kept at 800°C for 1 h. The carbonized mat was then treated with steam at 800°C for 30 min. The activated carbon mats with different coal ratios (PAN/coal = 5:0, 5:1, 5:3, 5:5) were denoted as PAN-AC, PAN-Coal-AC1, PAN-Coal-AC3, and PAN-Coal-AC5. The synthesis process of the CBACFs is presented in Fig. 1.

Structural Characterization

The morphology of the product was observed by scanning electron microscopy (SEM) on a Hitachi S-4800 scanning electron microscope with acceleration voltage of 5 kV. Energy dispersive X-ray spectroscopy (EDS) measurement was performed using a (TEAM™ EDS Analysis System). Infrared spectroscopy study was carried out using a Bruker VERTEX 70 Fourier transform infrared (FT-IR) spectrometer. Raman spectroscopy was performed on a Bruker SENTERRA dispersive Raman microscope using a 532 nm laser. The SSA and pore size of the ACFs were measured with a Micromeritics ASAP 2020 Surface Area and Porosimetry Analyzer. Powder X-ray diffraction (XRD) measurements were conducted on a Bruker D8 Advance Diffraction diffractometer in the 2θ range from 10° to 80°, with Cu K_α radiation (λ = 0.15405 nm) at 40 kV, 40 mA. The solubility of the coal was measured by dissolving an excess amount of coal in different solvents, followed by subtracting the residual mass from the initial mass.

Electrochemical Characterization

Each supercapacitor electrode was 1×1 cm^2 in size. They were produced by sandwiching an ACF mat between pieces of nickel foam, followed by pressing on a hydraulic press at 5 Mpa. The electrochemical tests were performed in a three-electrode cell, in which platinum foil and saturated calomel electrode (SCE) were used as counter and reference electrodes, respectively. Cyclic voltammetry (CV) and galvanostatic charge-discharge measurements were carried out on an electrochemical workstation (CHI660D, Shanghai Chenhua Device Company, China). The cycling performance of the electrode was evaluated on a Land battery measurement system. (CT2001A, Wuhan LAND Electronics Co., Ltd).

Results and Discussion

Structure Characterization

The coal used in the experiment was treated with acid in order to enhance the solubility. We investigated the solubility of the acid treated coal in different organic solvents and found that the polarity of the solvent played an important role in determining the solubility of the acid treated coal. As shown in Table 2, the acid treated coal dissolved well in polar solvents such as ethanol, acetone, and DMF; however, the acid treated coal was insoluble in non-polar and weak polar solvents such as toluene, CCl_4, and cyclohexane. The solubility of the coal increased with increasing solvent polarity. It can be seen from Table 2 that compared with

the other solvents, DMF was the best solvent for acid treated coal. As an additional advantage, DMF is also the solvent for PAN. Thus, we selected PAN/coal/DMF dispersion as the spinning dope.

Table 2 -Solubility of acid treated coal in different solvents.

Solvent	Cyclohexane	CCl_4	Toluene	Ethanol	Acetone	DMF
Polarity	0.1	1.6	2.4	4.3	5.4	6.4
Solubility of acid treated coal (g/ 100g)	0	0	0	2.1	4.7	6.6

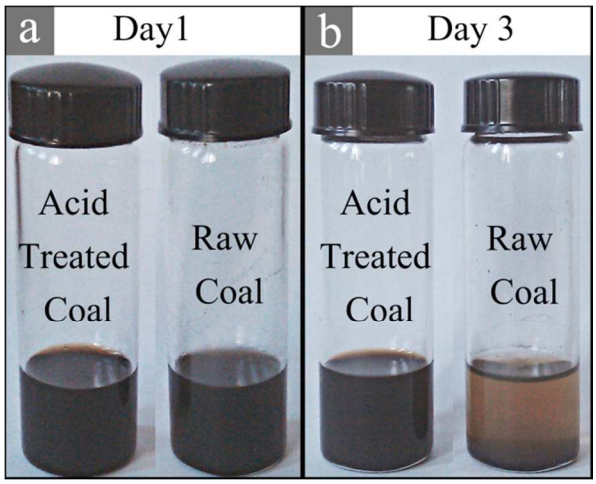

Fig. 2 Optical photographs of acid treated coal and raw coal dispersed in DMF: (a) Scintillation flasks containing raw coal/DMF and acid treated coal/DMF. (b) After standing for 3 days, the raw coal precipitated, while the acid treated coal/DMF dispersion remained homogeneous.

The acid treated coal showed different solubility in these solvents, and could reach a solubility as high as 6.6wt % in DMF. Fig. 2 presents optical photographs of the acid treated coal and the raw coal dispersed in DMF. After 3 days, the raw coal precipitated at the bottom of the scintillation flask, while the acid treated coal/DMF remained a homogeneous dispersion.

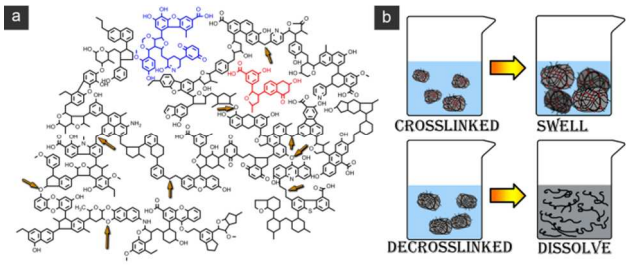

Fig. 3 (a) Molecular representation of coal proposed by Shinn[23]; the red and blue molecules represent the low molecular weight parts, and the arrows indicate the bonds that can be easily broken. (b) The cross-linked polymer network swells in solvent, while the de-crosslinked polymer chains dissolve in solvent.

The coal powders can be well dispersed in DMF after acid treatment. According to the coal model proposed by Marzec, the organic structure of coal consists of crosslinked macromolecule networks and relatively small molecules. The small molecule phase is clathrated in the macromolecule network[22]. This model can well explain the swelling of coal in solvents, which is a typical phenomenon for common cross-linked macromolecules. Another classical coal structure model derived from one-stage and two-stage coal liquefaction products was proposed by Shinn[23]. The Shinn model explains coal structure as an assembly of macromolecule units with different molecular weight, aromaticity, and functional groups connected by aliphatic and ether bonds. The Shinn model also contains a description of both the cross-linked macromolecule units and the relatively smaller molecules, although this model is focused more on the detailed chemical structures. It can be concluded from the Shinn model that the aliphatic or ether bonds are easily broken under harsh reaction conditions (Fig. 3). In this work, raw coal was treated by a mixture of sulfuric acid and nitric acid. The breaking of the aliphatic and ether bonds can be explained as follows: on the one hand, the sulfuric acid protonates the oxygen atoms in the ether bonds, and thus makes them even more vulnerable to attack by nucleophilic reagents such as nitro groups. On the other hand, the strong oxidative nitric acid could directly break the aliphatic bonds between the macromolecule units. Besides the reactions involving the bonds that connect these macromolecule units, the aromatic rings or aliphatic rings might be oxidized under these harsh reaction conditions and produce oxidative groups on the edges of the macromolecule units. The breaking of these bonds leaves the macromolecule units separated from each other. These separated macromolecule units with polar groups on their edges are much easier to disperse in solvent. The excellent dispersability of the acid treated coal can also be seen, as the de-crosslinked macromolecules dissolve rather than swell, unlike the cross-linked polymer networks in solvent.

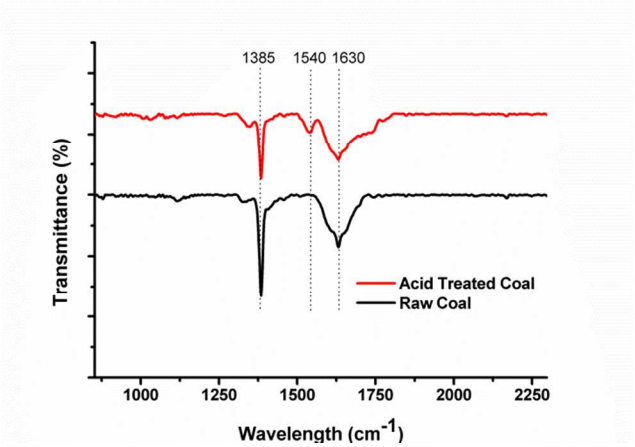

Fig. 4 FT-IR spectra of acid treated coal and raw coal.

The surface functional groups before and after the acid treatment were investigated by FT-IR spectroscopy. The characteristics peaks located at 1385 cm^{-1} and 1630 cm^{-1} were observed in both samples, which can be assigned to $–CH_3$ or $–C(CH_3)_3$ stretching vibrations and C=C stretching vibrations, respectively (Fig. 4).

The peak at 1540 cm^{-1} appeared after acid treatment, indicating that nitro groups were introduced by acid treatment. The band appeared between 1630-1700 cm^{-1} can be related to increased C=O groups after acid treatment. The nitro groups and oxygen groups offered strong polarity, which is a good agreement to the enhanced solubility of coal after acid treatment.

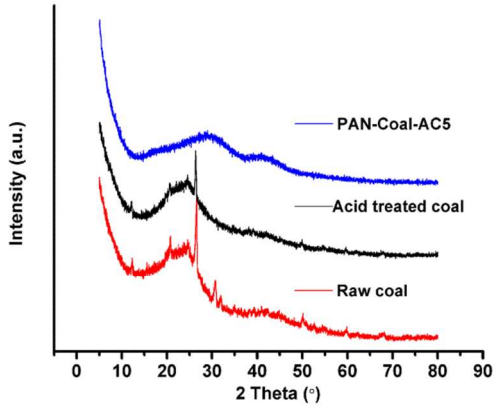

Fig. 5 XRD patterns of raw coal, acid treated coal, and CBACFs (PAN-Coal-AC5).

XRD patterns of the raw coal, acid treated coal, and CBACFs are shown in Fig. 5. It can be seen from the XRD patterns that all three samples exhibit the 002 reflection peaks of graphitic carbon around 26° and 43° (JCPDS 26-1079). All the peaks of the three samples are shifted due to the distortion of the lattice. The peaks of both the raw coal and the acid treated coal are shifted to lower angles compared to graphite, which may be attributed to the turbostratic structure of coal. The peaks of the CBACFs are shifted to a relatively high angle, which can be attributed to the decreased interlayer spacing d_{002} during carbonization. The reflection peaks of raw coal and acid treated coal are nearly identical, except that the peaks at 30° and 32° have disappeared for the acid treated sample, which can be attributed to the elimination of mineral components (e.g. dolomite (JCPDS 36-0426)) during acid treatment. The colour of ash changed from pink to white after acid treatment (Fig S1). This phenomenon is also an indirect proof of elimination of other mineral components. Analysis showed that the ash contents were 6.19% and 7.18% for the acid treated coal and raw coal, respectively (Table S1). The peak at 26° indicates the presence of SiO_2 (JCPDS 11-0252) in both the raw coal and the acid treated coal, but it disappears in the XRD pattern of the CBACF sample. The absence of SiO_2 in the CBACFs was due to the selection of the upper part of the solution as the spinning dope.

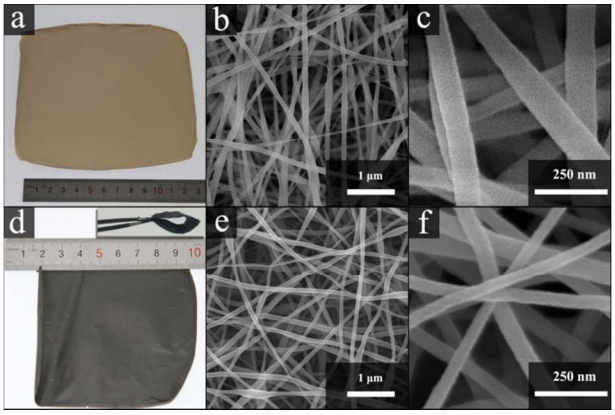

Fig.6 Optical images and SEM images of as-spun PAN-Coal-5 fibres and activated PAN-Coal-AC5 fibres: (a) Optical image of as-spun fibre mat. (b) SEM image of as-spun fibres at low magnification. (c) Magnified SEM image of as-spun fibres. (d) Optical image of CBACF mat (inset: piece of CBACF mat bent by tweezers). (e) SEM image of CBACFs at low magnification. (f) Magnified SEM image of CBACFs.

As shown in Fig. 6(a), the as-spun coal based fibre mats were dark brown, indicating that the coal was incorporated during spinning. We further carried out SEM to study the morphology of the products. The SEM image with low magnification [Fig. 6(b)] shows that the as-spun fibre mat is composed of continuous filaments. In the high magnification SEM image [Fig. 6(c)], the average diameter of the as-spun fibres is found to be around 100 nm. Fig. 6(d) shows an optical image of a CBACF mat, where the size of the mat has obviously decreased compared with the as-spun fibre mat before activation. The inset image of Fig. 6(d) is a piece of CBACF mat bent by tweezers. The CBACF mat shows quite good flexibility and mechanical strength, so that it has potential in applications of flexible devices. A low magnification SEM image of CBACFs is shown in Fig. 6(e). The fibres keep their continuous filament morphology after carbonization and activation, which is a result of the mild activation process and guarantees good mechanical strength on the macroscale. It can be seen from the magnified SEM image [Fig. 6(f)] that the average diameter of the CBACFs has shrunken to around 50 to 80 nm after carbonization and activation. The decrease in the diameter is related to the release of nitrogen and hydrogen in the cross-linking process of the polymer chains during carbonization. Thermogravimetric analysis showed that 47.7wt% of PAN and 51.4wt% of acid treated coal remained at 800°C (Fig. S1). The carbon content derived from acid treated coal was calculated to be 50.3wt% (see SI for more details).

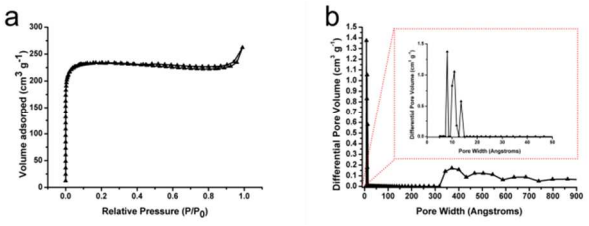

Fig.7 (a) BET isotherm and (b) pore size distribution of PAN-Coal-AC5 sample (Inset: detailed pore size distribution from 0 to 5 nm).

The SSA and the pore structure of the synthesized samples were determined by nitrogen adsorption/desorption isotherms. Table 3 summarizes the SSA values of samples with different coal content. The SSA values of the CBACFs, as determined by the Brunauer Emmett Teller (BET) method, increased with the coal content. The surface area of the CBACFs greatly increased for the PAN-Coal-AC5 sample, which might be attributed to the addition of a larger amount of coal. It can be concluded from the average pore size in Table 3 that the pore structure of the CBACFs mainly consists of micropores. Furthermore, the amount of micropores increases with the SSA, according to the ratio of the pore volume of the micropores to the total pore volume. Fig. 7(a) is the BET isotherm of the PAN-Coal-AC5 sample. The shape of the isotherm is that of a type I isotherm, which is more evidence for the microporosity of the CBACFs. Fig. 7(b) is the pore size distribution of the sample. The size range of micropores is mainly from 0.7 to 1.5 nm. The micropores were formed during the activation process and the interaction between the coal fragments and polymer chains during carbonization. The other set of peaks mainly fall into the range from 300 to 1000 nm. The macropores are mainly constructed by the intercrossed fibers.

Table 3 SSA and porosity of samples with different coal content.

Samples	S_{BET} [a] ($m^2\ g^{-1}$)	V_t [b] ($cm^3\ g^{-1}$)	V_{mic} [c] ($cm^3\ g^{-1}$)	V_{mic}/V_t [d] (%)	D_{ap} [e] (nm)
PAN-Coal-AC1	772	0.362	0.272	75	1.873
PAN-Coal-AC3	798	0.349	0.290	83	1.751
PAN-Coal-AC5	902	0.405	0.352	86	1.797

[a] SSA or BET specific surface area (S_{BET}). [b] Total pore volume (V_t) calculated at $P/P_0 = 0.99$. [c] Volume of micropores (V_{mic}) calculated by t-plot method. [d] Ratio of micropore volume to total volume. [e] Average pore size ($D_{ap} = 4V_t/S_{BET}$).

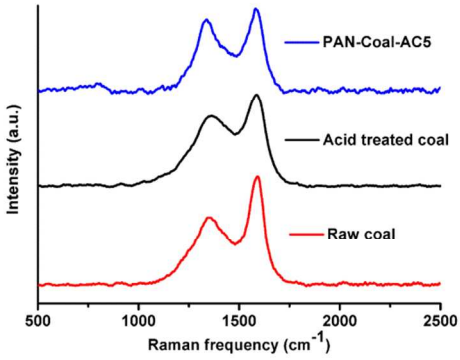

Fig.8 Raman spectra of CBACFs, acid treated coal, and raw coal.

Raman spectroscopy was adopted to study the degree of carbonization of the activated fibers, the acid treated coal, and the raw coal (Fig. 8). The peaks around 1600 and 1300 cm^{-1} are identified as the G peak and D peak, respectively. The intensity ratio of the G peak to the D peak, denoted as I_G/I_D, indicates the degree of graphitization of the carbon material. The I_G/I_D value increases with higher graphitic content, while it decreases with disorder in the carbon structure. The G peak at 1590 cm^{-1} corresponds to a splitting of the E_{2g} stretching mode of graphite and reflects the structural intensity of the sp^2-hybridized carbon atoms. The D peak at 1350 cm^{-1} is attributed to the vibrations of carbon atoms with dangling bonds in disordered graphite planes and in the defects incorporated into pentagon and heptagon graphite-like structures[24, 25]. The I_G/I_D ratios for raw coal, acid treated coal, and CBACFs were 1.59, 1.32, and 1.15, respectively. It can be inferred from the decreased I_G/I_D value that some of the lamellar structures of carbon layers in the raw coal were destroyed during the acid treatment. The I_G/I_D value further decreased for the CBACFs. This might be attributed to the activation reaction in which the surface carbon atoms were taken away, thus leaving dangling bonds at the surface and forming a disordered carbon structure.

Electrochemical characterization

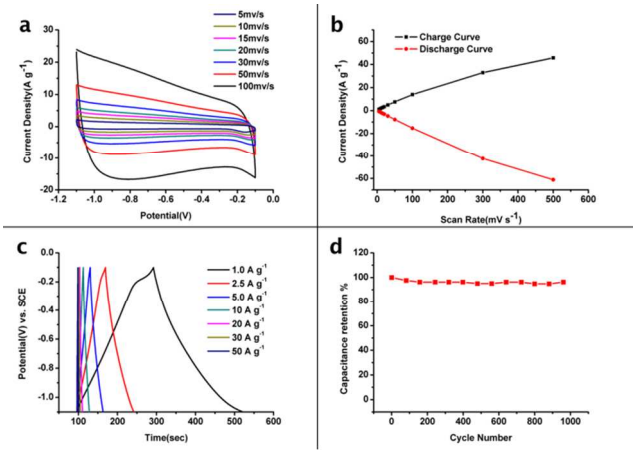

Fig. 9 Electrochemical performance of PAN-Coal-AC5 measured in a three-electrode system using 6 M KOH aqueous solution as electrolyte. (a) CV curves at scan rates from 5 to 100 mV s^{-1}. (b) Plot of current density versus scan rate. (c) Galvanostatic charge-discharge curves at different current densities ranging from 1 to 50 A g^{-1}. (d) Cycling performance of the PAN-Coal-AC5 electrode at 2 A g^{-1}.

In order to study the electrochemical performance, the CV response of the PAN-Coal-AC5 fibers was studied in 6 M KOH at potential intervals from -1.1 to -0.1 V vs. SCE. As can be seen in Fig. 9(a), the CV plot of PAN-Coal-AC5 shows a quasi-rectangular shape at different scan rates, indicating the EDL capacitive behavior of the coal based electrode. An obvious hump could be observed in the curve at the scan rate of 100 mV s^{-1}, which is caused by the redox reaction of oxygen groups on the electrode surface. The presence of oxygen groups also enhances the wettability of the electrode material and thus enlarges the contact area of the electrolyte and the electrode[3]. Fig. 9(b) presents the dependence of the current density (extracted from the

CV plot at 0.6 V) on the scan rate. The plot keeps a linear shape between 5-300 mV s^{-1}, while it exhibits a slightly compressed shape at 500 mV s^{-1} for both the charge and discharge processes. The near-linear shape indicates the high rate performance of the material due to ~~the high conductivity of the ACF mat and~~ the fast ion transportation in the micropores and mesopores formed by the fibers, and the fiber net provide an easily available electrode/electrolyte interface for forming an EDL[26]. Fig. 9(c) shows the galvanostatic charge-discharge curves of the PAN-Coal-AC5 fibers at various current densities. The quasi-triangular shape of the curves indicates an EDL response. There is a slight distortion of the curves caused by the pseudocapacitance of oxygen-groups, which is consistent with the shape of CV curves. The specific capacitance of the electrode was calculated by Eq. (1):

$$C_s = \frac{I\Delta t}{m\Delta V} \quad (1)$$

Where I, Δt, m, and ΔV are the applied current, discharge time, mass of the active material, and the voltage change, respectively. The specific capacitance of PAN-Coal-AC5 was calculated to be 230 F g^{-1} at the current density of 1 A g^{-1} according to Eq. (1). Capacitance retention of the electrode is shown in Fig. 9(d). The 97% of its initial capacitance was retained after 1000 cycles at the current density of 2 A g^{-1}. The excellent cycling stability is mainly attributed to the EDL capacitive behavior of the electrode and the small weight loss during the cycling guaranteed by well contact of coalesced fibers and the electrode[13].

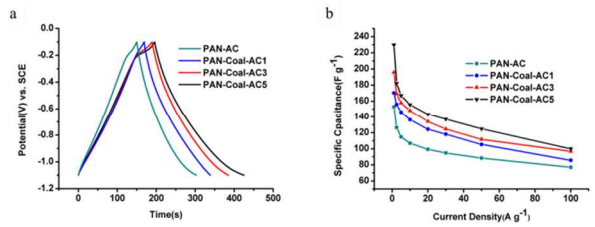

Fig. 10 Electrochemical performance of activated carbon fibers with various coal ratios. (a) Galvanostatic charge-discharge curves of samples at the current density of 1 A g^{-1}. (b) Specific capacitance of samples versus various current densities from 1 to 100 A g^{-1}.

We also performed electrochemical tests on the samples with various coal ratios for comparison. Fig. 10 presents the electrochemical performances of PAN-Coal-AC5, PAN-Coal-AC3, PAN-Coal-AC1, and PAN-AC. The galvanostatic charge-discharge curves at 1 A g^{-1} of the samples with various coal contents are shown in Fig. 10(a). The specific capacitance of the samples increased with the coal content. The specific capacitance of PAN-Coal-AC5 was 230 F g^{-1}, while the ACFs derived from pure PAN showed a relative low specific capacitance of 153 F g^{-1}. The enlarged capacitance was due to the enlargement of the SSA and the increase in oxygen groups when coal was added. EDS analysis of carbon/oxygen ratio showed that there was an increase of oxygen content when acid treated coal was introduced (Table S3). Also the FT-IR results showed the increase of surface functional groups. The acid treated coal is a material with a low degree of graphitization, so that it is easier to activate[17]. Furthermore, the coal fragments are intercalated into the PAN molecules, which hinder the cross-linking between macromolecules during carbonization and thus create pores. The different carbon yields of the two components in the fibers might also have played a role in creating pores. This hypothesis was justified by the enhanced capacitance of the coal-based carbon fibers without activation (Table 4). The capacitance of these fiber mats increased with increasing coal content as well. The capacitance of un-activated carbon fibers with coal/PAN ratios of 0:1, 1:5, 3:5, and 5:5 were 82.3 F g^{-1}, 148.8 F g^{-1}, 155.4 F g^{-1}, and 177.2 F g^{-1} at the current density of 1 A g^{-1}, respectively. The results imply that activation is not the only process in creating pores in the fibers; coal might also take a part in developing pores. Fig. 10(b) shows the effect of current density on the specific capacitance of electrodes with various coal ratios. It can be seen that the specific capacitance of the CBACF samples with higher coal content is larger than for those with lower coal content at each current density. The specific capacitance of PAN-Coal-AC5 was 100 F g^{-1} at the current density of 100 A g^{-1}, while the capacitance dropped to 77 F g^{-1} at 100 A g^{-1} for the coal-free sample (PAN-AC). We believe that with increasing amount of acid treated coal, the content of low graphitization carbon also increased. These turbostratic carbon segments collapse during carbonization and pores are created. The excellent rate performance was due to the fibrous morphology of the samples, which enabled the fast transportation of electrolyte and efficient ion diffusion[4].

In summary, we believe that there are mainly three contributions to the increase of capacitance with increasing amount of coal. Firstly, with more acid treated coal, more pores will form due to the collapse of turbostratic carbon and release of gases during carbonization. Secondly, the coal fragments prevent PAN molecule from interconnection under high temperature. Finally, the carbon yields of acid treated coal and PAN are different, which leads to the formation of cavities in the resulting carbon fibers.

Table 4 Specific capacitance of samples at the current density of 1 A g^{-1}

Samples	PAN-AC	PAN-Coal-AC1	PAN-Coal-AC3	PAN-Coal-AC5	PAN-C	PAN-Coal-1	PAN-Coal-3	PAN-Coal-5
Capacitance (F g^{-1})	153.0	170.2	195.6	230.0	82.3	148.8	155.4	177.2

Conclusions

We have prepared coal-based carbon nanofiber mats by electrospinning PAN/coal dispersion. The dissolution of acid treated coal in polar organic solvent was explained as due to the acid treatment, which breaks the weak bonds between macromolecular units in the coal structure. The porosity of the CBACFs can be controlled by varying the coal content in the precursor dispersion. The CBACFs can be used as supercapacitor electrode and featured excellent electrochemical performances. The CBACF electrode showed a capacitance of 230 F g^{-1} at the current density of 1 A g^{-1}, and kept 97% of its initial capacitance after 1000 cycles at the current density of 2 A g^{-1}. The assembly of such electrodes is free of binders and conductive agents, which greatly simplifies the preparation of electrodes. The electrospinning process for preparing coal-based carbon nanofibers features low energy consumption compared to the conventional ways of breaking coal down to the nanoscale, so that it is more applicable to industrial production than previous methods.

Acknowledgements

This work is supported by the Xinjiang Autonomous Region Major Projects (No. 201130113-1) and the National Science Foundation of China (No. U1203292)

Notes and references

[a] *Key Laboratory of Material and Technology for Clean Energy, Ministry of Education; Key Laboratory of Advanced Functional Materials,; Institute of Applied Chemistry, Xinjiang University. Urumqi 830046, Xinjiang Autonomous Region, P.R. China.; E-mail: jdz@xju.edu.cn*

[b] *Laboratory of Industrial Chemistry, Ruhr University Bochum, 44780 Bochum, Germany; E-mail: wei.xia@techem.rub.de*

c. Institute for Superconducting & Electronic Materials, University of Wollongong, NSW 2522, Australia

† Dedicated to Professor Xinquan Xin on the occasion of his 80th birthday.

‡ Electronic Supplementary Information (ESI) available: Ash content anaylsis of acid treated coal, calculation of mass ratio, and the EDS analysis.

References

1 Gryglewicz G, Machnikowski J, Lorenc-Grabowska E, Lota G, Frackowiak E, *Electrochimi. Acta*. , 2005;**50**(5):1197-206.
2 Hao L, Li X, Zhi L, *Adv. Mater*., 2013;**25**(28):3899-904.
3 Conway BE. *Electrochemical supercapacitors: Scientific fundamentals and technological applications.* 1st ed. New York: Kluwer Academic Plenum Publishers; 1999: 6-7.
4 Yun YS, Im C, Park HH, Hwang I, Tak Y, Jin H-J, *J. Power Sources*, 2013;**234**(0):285-91.
5 Ji L, Lin Z, Medford AJ, Zhang X. *Carbon.* 2009;**47**(14):3346-3354.
6 Ji L, Zhang X. *Electrochem. Commun.* 2009;**11**(3):684-687.
7 Ji L, Lin Z, Alcoutlabi M, Zhang X. *Energ. Environ. Sci.* 2011;**4**(8):2682-2699.
8 Ji L, Rao M, Aloni S, Wang L, Cairns EJ, Zhang Y. *Energ. Environ. Sci.* 2011;4(12):5053-5059.
9 Ji L, Medford AJ, Zhang X. *J. Polymer Sci. B Polymer Phys*. 2009;**47**(5):493-503.
10 Liwen J, Xiangwu Z. *Nanotechnology*. 2009;**20**(15):155705.
11 Merino C, Soto P, Vilaplana-Ortego E, Gomez de Salazar JM, Pico F, Rojo JM, *Carbon*, 2005;**43**(3):551-7.
12 Chen L-F, Huang Z-H, Liang H-W, Guan Q-F, Yu S-H, *Adv.Mater.*, 2013;**25**(34):4746-52.
13 Li Z, Zhang L, Amirkhiz BS, Tan X, Xu Z, Wang H, et al., *Adv. Energy Mater.*, 2012;**2**(4):431-7.
14 Liang Y, Wu D, Fu R, *Sci. Rep*., 2013;**3**:1119.
15 Bao L, Li X, *Adv. Mater.*, 2012;**24**(24):3246-52.
16 Park SH, Kim C, Choi YO, Yang KS. ,*Carbon*, 2003;**41**(13):2655-7.
17 Xu B, Wu F, Chen S, Zhang C, Cao G, Yang Y, *Electrochimi. Acta*., 2007;**52**(13):4595-8.
18 Qiu JS, Li YF, Wang YP, Wang TH, Zhao ZB, Zhou Y, et al., *Carbon*, 2003;**41**(11):2170-3.
19 Li Z, Hu C, Yu C, Adams H, Qiu J ,*Carbon*, 2010;**48**(7):1926-31.
20 Greiner A, Wendorff JH, *Angew. Chem. Int. Ed.*, 2007;**46**(30):5670-703.
21 Zhao Y, Wu J, Wang N, Jiang L, *J. Mater. Chem. A*, 2013;**1**(25):7290-305.
22 Marzec A, *Fuel Process. Technol.*, 1986;**14**(0):39-46.
23 Shinn JH, *Fuel*., 1984;**63**(9):1187-96.
24 Dresselhaus MS, Dresselhaus G, Saito R, Jorio A, *Phys. Rep.*, 2005;**409**(2):47-99.
25 Li H, Kang W, Wang L, Yue Q, Xu S, Wang H, et al., *Carbon*, 2013;**54**:249-57.
26 Kim C, Ngoc BTN, Yang KS, Kojima M, Kim YA, Kim YJ, et al. *Adv. Mater.* 2007;**19**(17):2341-2346.